

Be Careful When Evaluating Explanations Regarding Ground Truth

Hubert Baniecki^{1*}, Maciej Chrabaszcz^{2*},
Andreas Holzinger^{3,4}, Bastian Pfeifer⁴, Anna Saranti³, Przemyslaw Biecek^{1,2}

¹MI2.AI, University of Warsaw, Poland ²MI2.AI, Warsaw University of Technology, Poland

³Human-Centered AI Lab, University of Natural Resources and Life Sciences Vienna, Austria

⁴Medical University of Graz, Austria
{h.baniecki, p.biecek}@uw.edu.pl

Abstract

Evaluating explanations of image classifiers regarding ground truth, e.g. segmentation masks defined by human perception, primarily evaluates the quality of the models under consideration rather than the explanation methods themselves. Driven by this observation, we propose a framework for *jointly* evaluating the robustness of safety-critical systems that *combine* a deep neural network with an explanation method. These are increasingly used in real-world applications like medical image analysis or robotics. We introduce a fine-tuning procedure to (mis)align model–explanation pipelines with ground truth and use it to quantify the potential discrepancy between worst and best-case scenarios of human alignment. Experiments across various model architectures and post-hoc local interpretation methods provide insights into the robustness of vision transformers and the overall vulnerability of such AI systems to potential adversarial attacks.

1 Introduction

“One should keep in mind that a heatmap always represents the classifier’s view, i.e., explanations neither need to match human intuition nor focus on the object of interest.” – Samek et al. (2016)

Evaluating explanations of (deep) machine learning models is at the forefront of the current discourse about their trustworthiness in many critical applications, including medical imaging (Arun et al. 2021). One suggests we could omit using opaque models for high-stakes decision-making like medical diagnosis (Rudin 2019), yet deep learning continues to achieve great performance in classifying diseases from unstructured data. A valid concern raised by physicians is the importance of prediction consistency, i.e. features coming from different modalities (not only images) may be a requirement for an accurate assessment of the patient’s outcome (Holzinger, Haibe-Kains, and Jurisica 2019).

With that in mind, a popular approach to interpreting decisions of deep neural networks is local post-hoc explanations (Guidotti et al. 2020; Shrotri et al. 2022; Joo et al. 2023), which cannot be adopted in practice without them being evaluated properly. Unfortunately, evaluating explanations becomes challenging for multiple reasons: (i) lack of ground truth (Guidotti 2021; Zhou et al. 2022; Agarwal et al. 2022),

(ii) different goals achieved by various explanation algorithms and evaluation metrics (Tomsett et al. 2020; Bhatt, Weller, and Moura 2020; Dai et al. 2022; Komorowski, Baniecki, and Biecek 2023), (iii) spurious correlations and confounding features in datasets (Adebayo et al. 2022), (iv) human perception bias (Arora et al. 2022), (v) **no clear distinction between evaluating explanations and model behaviour**. The latter is a particular focus of this paper.

In line with these concerns, Saporta et al. (2022) introduces the first human benchmark for chest X-ray segmentation in a multilabel classification set-up. Their presented work claims to allow demonstrating low alignment of popular explanation methods like Grad-CAM (Selvaraju et al. 2019) with human perception. In this paper, we aim to emphasize that evaluating explanations regarding ground truth may primarily demonstrate low localization performance of deep learning models instead.

Contribution. We first show an intuitive example where evaluating explanation methods regarding ground truth is not robust and needs to be done with caution (Section 2). Motivated by this insight, we introduce a novel framework for *jointly* evaluating the robustness of AI systems defined as a *combination* of a deep learning model with an explanation method, which takes into account the alignment between AI systems and human experts (Section 3). Using a recent real-world medical use case, we validate our framework in extensive experiments including convolutional neural networks and vision transformers combined with post-hoc local interpretation methods (Section 4). We conclude with a discussion on related work and broader impact (Section 5).

2 Motivation: The Case of Interpreting Chest X-ray Classification

To illustrate a typical pitfall in evaluating explanations, we show that benchmarking their localization property regarding ground truth can be ambiguous. Specifically, such a result effectively serves as a benchmark for a *model–explanation pipeline*, not necessarily explanation methods. We consider a case of interpreting a model for classifying lung pathologies in chest X-ray images. Following the experimental setup described in (Saporta et al. 2022), we train a DenseNet-121 model (Huang et al. 2019) on the CheXpert dataset to classify 14 lung pathologies.

*These authors contributed equally.

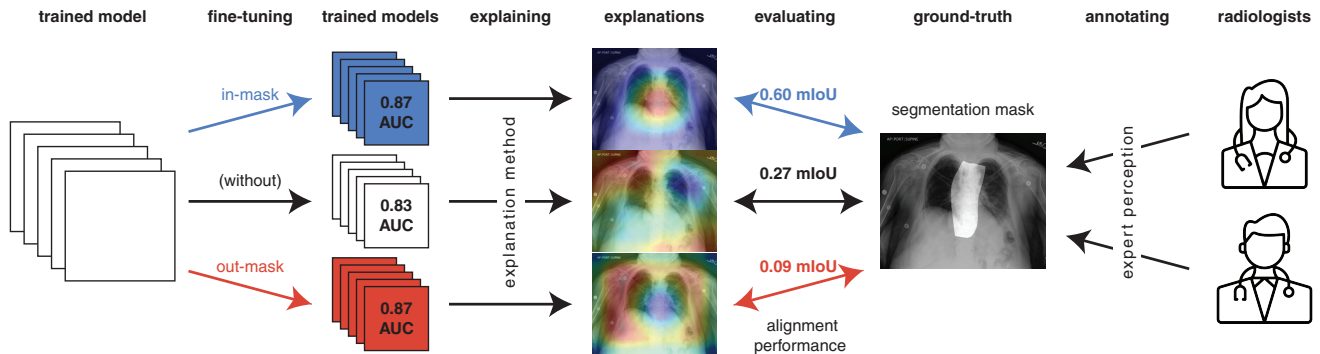


Figure 1: Evaluating explanations regarding ground truth, e.g. segmentation masks defined by human perception, is not robust. It primarily evaluates the quality of the combined model–explanation pipeline.

Pathology: Atelectasis					
Model	AUC \uparrow	MI \uparrow	Explanation	Hit-rate \uparrow	mIoU \uparrow
DenseNet	0.84	0.18	Grad-CAM	0.11	0.08
DenseNet + in-mask	0.84	0.15	Grad-CAM	0.58 (+0.47)	0.28 (+0.20)
DenseNet + out-mask	0.83	0.18	Grad-CAM	0.03 (−0.08)	0.07 (−0.01)

Pathology: Enlarged Cardiomeastinum					
Model	AUC \uparrow	MI \uparrow	Explanation	Hit-rate \uparrow	mIoU \uparrow
DenseNet	0.83	0.21	Grad-CAM	0.36	0.27
DenseNet + in-mask	0.87	0.28	Grad-CAM	0.93 (+0.57)	0.60 (+0.33)
DenseNet + out-mask	0.87	0.24	Grad-CAM	0.00 (−0.36)	0.09 (−0.18)

Table 1: Comparison between different DenseNet models fine-tuned on two predictive tasks achieving similar predictive performance measured with AUC and mutual information (MI). The models differ in alignment performance measured with Hit-rate and mIoU, which is an intersection between explanations produced by Grad-CAM and a ground truth annotated by humans.

We then modify the model by fine-tuning it on the test set of CheXlocalize,¹ which includes ground truth masks of lung pathologies. It is done in a way to impact the localization of explanations using regularization (similarly to Heo, Joo, and Moon 2019). For a concise example, we select the Grad-CAM explanation method and two pathologies: *atelectasis* and *enlarged cardiomeastinum*, but note that other explanations and class labels can be used as well.

Table 1 shows the result of our experiment where we fine-tune the model in two different ways: the first approach modifies a loss function to align the explanations with the ground-truth mask (labelled with *in-mask*), and the second modifies the loss function to encourage explanations pointing outside the mask (*out-mask*). We could demonstrate that DenseNet achieves comparable predictive performance (AUC and mutual information) on the validation set but **very different alignment performance between the three scenarios** (Hit-rate and mIoU as defined by Saporta et al. 2022). The results highlight the pivotal safety issue in evaluating explanation methods regarding ground truth (see Figure 1).

¹CheXlocalize is originally split into test and validation sets; we use the latter for evaluation (see Appendix A for details).

3 Framework for Evaluating the Robustness of Model–Explanation Pipelines

We now introduce a refined framework for evaluating the robustness of AI systems, which deal with human-aligned classification by *combining* a deep learning model with an explanation method (in short: model–explanation pipelines).

Background on explanation methods

We consider a classification setup where an explanation of the model’s prediction is given by feature attribution scores. For the purpose of this work, we chose four widely-adopted explanation methods for deep learning models: Vanilla Gradient (VG, Simonyan, Vedaldi, and Zisserman 2014), Integrated Gradients (IG, Sundararajan, Taly, and Yan 2017), SmoothGrad (SG, Smilkov et al. 2017) and Layer-wise Relevance Propagation (LRP, Bach et al. 2015). We excluded Grad-CAM as it is specific to convolutional neural networks, and we aim to include a vision transformer (ViT, Dosovitskiy et al. 2021) in experiments (Section 4).

Let f be a differentiable model and g be an explanation method. Then, explanation E for input x can be defined as $E = g(f, x)$ where it targets a single predicted class.

VG explanation method computes the gradient of inputs with respect to the model’s output: $g_{\text{VG}}(f, x) := \frac{\partial f(x)}{\partial x}$. IG improves its faithfulness by computing the integral (sum) of such gradients with respect to the linear combination of input x and baseline x' , e.g. a black image, for all features:

$$g_{\text{IG}}(f, x, x') := (x - x') \cdot \frac{1}{n} \sum_{i=1}^n g_{\text{VG}}(f, x' + \frac{i}{n} \cdot (x - x')). \quad (1)$$

SG aims to improve the explanation’s stability by computing multiple (n) VG explanations around input x , e.g. by adding Gaussian noise $\mathcal{N}(0, \sigma^2)$ to it, and then aggregating these explanations with mean:

$$g_{\text{SG}}(f, x, n, \sigma^2) := \frac{1}{n} \sum_{i=1}^n g_{\text{VG}}(f, x + \mathcal{N}(0, \sigma^2)). \quad (2)$$

LRP considers the layer-wise structure of neural networks to determine feature attribution scores. Given the relevance $r_j^{(l+1)}$ of neuron j at layer $l + 1$, LRP decomposes $r_j^{(l+1)}$ into messages $r_{i \leftarrow j}^{(l, l+1)}$ from neuron i at layer l sent to neuron j of layer $l + 1$ so that the following holds: $r_j^{(l+1)} = \sum_{i \in (l)} r_{i \leftarrow j}^{(l, l+1)}$ and $r_i^{(l)} = \sum_{j \in (l+1)} r_{i \leftarrow j}^{(l, l+1)}$.

Bach et al. (2015) propose various rules for computing messages $r_{i \leftarrow j}^{(l, l+1)}$. One of the most common is ϵ -rule using $z_j = \sum_i z_{ij}$ to compute:

$$r_{i \leftarrow j}^{(l, l+1)} = \frac{z_{ij}}{z_j + \epsilon \cdot \text{sign}(z_j)} r_j^{(l+1)}. \quad (3)$$

The final explanation consists of the relevance scores of features from the first layer $g_{\text{LRP}}(f, x, \epsilon) := r^{(1)}(f, x, \epsilon)$.

Measuring human-aligned classification

We define *alignment* between an AI system and humans as an intersection between model explanations and the ground-truth region of interest. To measure how well the model explanation E aligns with the corresponding binary mask M , e.g. a segmentation mask created by a human expert, we use two intuitive accuracy metrics widely used in explainability research (Arras, Osman, and Samek 2022):

$$\mathcal{D}_{\text{mass}}(E, M) := \frac{\sum_{i \in M_{\perp}} E_i}{\sum_i E_i}, \quad (4)$$

where $M_{\perp} = \{i : M_i = 1\}$ is a set of feature indices, and

$$\mathcal{D}_{\text{rank}}(E, M) := \frac{|\{i : i \in M_{\perp} \wedge i \in E_{\perp k}\}|}{k}, \quad (5)$$

where $k = |M_{\perp}|$ denotes the size of set M_{\perp} and $E_{\perp k}$ represents the set of feature indices with k highest values in E .

(Mis)Aligning explanations with ground truth

To align the model–explanation pipelines with ground-truth masks, we fine-tune them with a differentiable alignment loss defined as:

$$\mathcal{L}_{\text{align}}(f, g, X) := \frac{1}{n} \sum_{x \in X} \|g(f, x)_{[0,1]} - M(x)\|^2, \quad (6)$$

where X is a set of n inputs corresponding to the ground-truth class of interest, M now varies depending on input x , and $g(f, x)_{[0,1]}$ denotes min-max scaling to ensure that explanation values correspond to binary values in the mask. We moreover clip negative feature attributions to 0 before computing the loss as positive attributions are associated with influencing the predicted class. The final fine-tuning loss function controls for change in model performance:

$$\mathcal{L}(f, g, X) = \mathcal{L}_{\text{cross-entropy}}(f, X) + \alpha \cdot \mathcal{L}_{\text{align}}(f, g, X), \quad (7)$$

where α is responsible for balancing the degree of model–explanation alignment. We found $\alpha = 1$ to be sufficient in our experiments (see e.g. Table 1).

Note that in a multi-label classification setup, each input can have multiple ground-truth masks corresponding to different classes. It is possible to extend $\mathcal{L}_{\text{align}}$ to additionally sum over a particular set of class labels.

Fine-tuning the model with $\mathcal{L}_{\text{align}}$ aligns its explanations with ground truth. We moreover consider *misaligning* model–explanation pipelines, which can be defined as predicting outside of ground truth. To do so, we invert binary masks and fine-tune the model accordingly:

$$\mathcal{L}_{\text{misalign}}(f, g, X) := \frac{1}{n} \sum_{x \in X} \|g(f, x)_{[0,1]} - (\mathbb{1} - M(x))\|^2. \quad (8)$$

Misalignment can be an issue whenever we consider an adversary attacking the AI system. Measuring misalignment gives us an intuition about the possible worst-case scenario corresponding to robustness.

Robustness of model–explanation pipelines

To investigate the robustness, we propose quantifying the difference in alignment accuracy for an aligned and misaligned model–explanation pipeline (f, g) defined as:

$$\mathcal{R}(f, g, X) := \frac{1}{n} \sum_{x \in X} \left[\mathcal{D}(g(f_{\text{align}}, x)_{[0,1]}, M(x)) - \mathcal{D}(g(f_{\text{misalign}}, x)_{[0,1]}, M(x)) \right], \quad (9)$$

where $f_{(\text{mis})\text{align}} = \text{argmin}_f \mathcal{L}_{(\text{mis})\text{align}}(f, g, X)$ is found with fine-tuning and \mathcal{D} measures mass or rank accuracy for the (mis)aligned model–explanation pipeline. This measures the expected difference between the best and worst-case scenarios in the sense of alignment with the ground-truth masks. Moreover, we consider fitting a linear regression model on differences under the sum in $\mathcal{R}(f, g, X)$ to find significant influence of various model architectures and explanation methods on the robustness of model–explanation pipelines.

4 Experiments

In experimental evaluation, we rely on the introduced framework to answer the following research questions (RQ) that are of interest to the potential developers and users of safety-critical AI systems:

- **RQ1:** How robust are convolutional neural networks and vision transformers in combination with various explanation methods?

- **RQ2:** What is the impact of (mis)aligning explanations on the model’s predictive performance?
- **RQ3:** Does pre-training a model on a similar dataset improve the robustness of model–explanation pipelines?
- **RQ4:** Are model–explanation pipelines equally robust across different class labels of interest?

Setup

Dataset. Following the motivational example described in Section 2, we use the CheXpert dataset (Irvin et al. 2019) for experiments. Our use-case of aligning the safety-critical system relies on the recently published CheXLocalize dataset (Saporta et al. 2022). It consists of 902 X-ray images with 10 multi-label classes, for which there are ground-truth masks generated by expert radiologists (see Figure 2). Details of the datasets and splits into subsets are available in Appendix A. Focusing on this real-world application allows us to maintain a reasonable amount of computation when comparing 12 different model–explanation pairs.

Models. We compare three deep neural network architectures: DenseNet-201 (Huang et al. 2019), ViT-base (Dosovitskiy et al. 2021) and Swin-ViT-base (Liu et al. 2021). We first train each model architecture on CheXpert with four types of weight initialization: (i) random initialization with 1 channel input, (ii) random initialization with 3 channel inputs (repetitions of a grey image), (iii) weights from a model pre-trained on the ImageNet-21k dataset (Ridnik et al. 2021), and (iv) weights from a model pre-trained on RadImageNet (Mei et al. 2022). Further training details are available in Appendix A.

We evaluate each model with macro AUROC, which is a default performance measure for multi-label classification. In Table 2, we can see that DenseNet outperformed transformer-based models in all types of initialization in terms of macro AUROC. Since for all three model architectures, random initialization with 3 channels gives better results than using only 1 channel, and pre-training on RadImageNet outperforms pre-training on ImageNet-21k, we further consider only those two superior types of initialization.

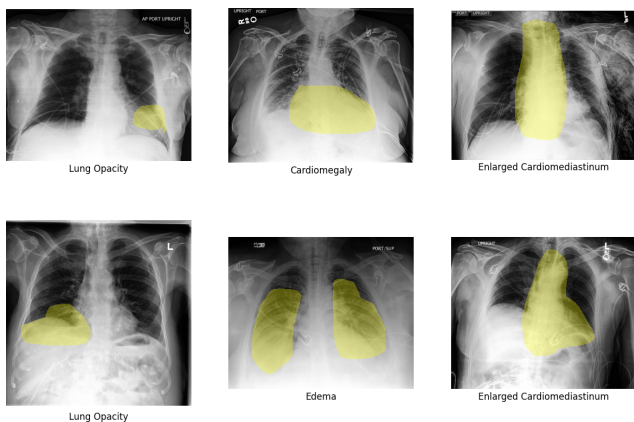


Figure 2: Example images with ground-truth masks related to labels generated by expert radiologists in CheXLocalize.

Initialization type	DenseNet	ViT	Swin-ViT
Random with 1 channel	0.729	0.694	0.688
Random with 3 channels	0.761	0.734	0.758
Pre-trained on ImageNet-21k	0.747	0.738	0.710
Pre-trained on RadImageNet	0.772	0.749	0.758

Table 2: Macro AUROC performance between the models.

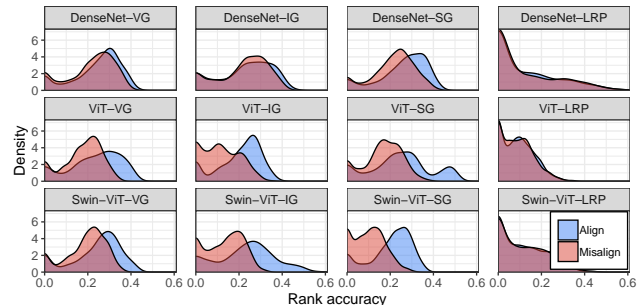


Figure 3: Distribution of *rank accuracy* values for the *pre-trained* model–explanation pipelines. For clarity, the x-axis is truncated from 1.0 to 0.6.

Explanations. On top of each model architecture, we add each explanation method (VG, IG, SG, LRP) described in Section 3. Explanation methods use default parameters, i.e. $x' = \emptyset$, $n = 20$, $\sigma = 0.1$, $\epsilon = 1e-6$. We fine-tune 12 model–explanation pipelines for (mis)alignment controlling for pre-training on RadImageNet. Each pipeline was fine-tuned with both \mathcal{L}_{align} and $\mathcal{L}_{misalign}$ for 25 epochs on the test set of CheXLocalize, which consists of 668 images with 10 annotated lung pathologies (class labels). Finally, for each scenario, we compute the described measures to evaluate both alignment and robustness. For simplicity, we fine-tune each pipeline considering only a single label at a time, and aggregate evaluation measures over classes.

Results

We first use all metadata to perform a sanity check for the consistency between values of mass and rank accuracy metrics under both alignment scenarios in Table 3. There is a relatively high correlation between \mathcal{D}_{mass} and \mathcal{D}_{rank} when computed for the same alignment scenarios (top rows). For each metric, there is an evident relationship between alignment accuracy for f_{align} and $f_{misalign}$ (middle rows). We further report the correlation between disjoint pairs of measures and models for completeness (bottom rows).

RQ1: How robust are convolutional neural networks and vision transformers combined with various explanation methods? Figure 3 shows the distribution of rank accuracy for both aligned and misaligned pipelines. There are visible differences in rank accuracy values, e.g. for DenseNet–SG, ViT–IG, and Swin-ViT–VG. We report analogous results for mass accuracy and non-pre-trained models in Appendix B. Detailed visual analysis can be more informative than aggregated metric values, e.g. in the case

Correlation between alignment metric values	Pearson	Spearman
$\mathcal{D}_{\text{mass}}(g(f_{\text{align}}, x)_{[0,1]}, M(x)) \times \mathcal{D}_{\text{rank}}(g(f_{\text{align}}, x)_{[0,1]}, M(x))$	0.887	0.920
$\mathcal{D}_{\text{mass}}(g(f_{\text{misalign}}, x)_{[0,1]}, M(x)) \times \mathcal{D}_{\text{rank}}(g(f_{\text{misalign}}, x)_{[0,1]}, M(x))$	0.867	0.919
$\mathcal{D}_{\text{mass}}(g(f_{\text{align}}, x)_{[0,1]}, M(x)) \times \mathcal{D}_{\text{mass}}(g(f_{\text{misalign}}, x)_{[0,1]}, M(x))$	0.614	0.715
$\mathcal{D}_{\text{rank}}(g(f_{\text{align}}, x)_{[0,1]}, M(x)) \times \mathcal{D}_{\text{rank}}(g(f_{\text{misalign}}, x)_{[0,1]}, M(x))$	0.634	0.696
$\mathcal{D}_{\text{rank}}(g(f_{\text{align}}, x)_{[0,1]}, M(x)) \times \mathcal{D}_{\text{mass}}(g(f_{\text{misalign}}, x)_{[0,1]}, M(x))$	0.572	0.703
$\mathcal{D}_{\text{mass}}(g(f_{\text{align}}, x)_{[0,1]}, M(x)) \times \mathcal{D}_{\text{rank}}(g(f_{\text{misalign}}, x)_{[0,1]}, M(x))$	0.606	0.654

Table 3: Consistency between values of alignment metrics for different scenarios measured with correlation. Pearson correlation measures the linear relationship between the two variables. Spearman rank correlation between two variables is equal to the Pearson correlation between the rank values of those two variables, which might be more appropriate to consider in this context.

Pre-trained	Model	Explanation	AUC _{align}	AUC _{misalign}	$\mathcal{R}_{\text{mass}}$	$\mathcal{R}_{\text{rank}}$
✗	DenseNet	VG	0.723	0.730	0.049	0.058
		IG	0.759	0.605	0.014	0.012
		SG	0.646	0.616	0.043	0.037
		LRP	0.707	0.762	0.002	0.005
	ViT	VG	0.722	0.681	0.046	0.040
		IG	0.742	0.679	0.062	0.045
		SG	0.744	0.663	0.069	0.064
		LRP	0.600	0.503	0.013	0.010
	Swin-ViT	VG	0.713	0.744	0.035	0.028
		IG	0.741	0.734	0.157	0.183
		SG	0.724	0.723	0.174	0.243
		LRP	0.778	0.752	–	–
✓	DenseNet	VG	0.802	0.762	0.033	0.026
		IG	0.749	0.732	0.018	0.010
		SG	0.793	0.680	0.060	0.046
		LRP	0.764	0.735	−0.002	−0.003
	ViT	VG	0.686	0.690	0.080	0.059
		IG	0.679	0.713	0.098	0.086
		SG	0.677	0.675	0.096	0.082
		LRP	0.611	0.490	0.005	0.002
	Swin-ViT	VG	0.705	0.756	0.069	0.050
		IG	0.728	0.701	0.118	0.100
		SG	0.748	0.704	0.094	0.101
		LRP	0.719	0.697	−0.005	−0.001

Table 4: Evaluating the robustness of AI systems that combine a deep learning model with an explanation method. We report predictive performance (macro AUROC) for aligned and misaligned pipelines, as well as their robustness measured based on values of rank and mass alignment metrics.

	Coef.	Std. Err.	p -value
intercept	0.024	0.0027	$8.1e-19$
pre-trained model	-0.003	0.0021	0.15
model: ViT	0.031	0.0025	$< 2.0e-32$
model: Swin-ViT	0.058	0.0026	$< 2.0e-32$
explanation: IG	0.026	0.0028	$1.2e-19$
explanation: SG	0.038	0.0028	$< 2.0e-32$
explanation: LRP	-0.044	0.0031	$< 2.0e-32$

Table 5: Coefficients of a linear regression model fitted to the differences of *mass accuracy* between aligned and misaligned model–explanation pipelines.

of ViT-SG, the distribution is bi-modal. Still, it becomes challenging to compare dozens of methods in practice. In Table 4, we report the robustness of all fine-tuned model–explanation pipelines. It can serve as a benchmark for evaluating the vulnerability of human-aligned classification. We acknowledge that the fine-tuning optimization task for LRP performed poorly as judged by the presented results, e.g. it did not converge in the case of non-pre-trained Swin-ViT. Future work can consider an extension of LRP customized to transformers (Ali et al. 2022).

RQ2: What is the impact of (mis)aligning explanations on the model’s predictive performance? Developers of safety-critical AI systems are interested in predictive performance. Table 4 includes macro AUROC values for both aligned and misaligned model–explanation pipelines. Some pairs exhibit no predictive performance change between the two scenarios, which might be worrisome for the end-user, granted there was a high difference between alignment performance. For example, Swin-ViT-SG has zero difference in AUROC, but relatively large robustness metric values.

RQ3: Does pre-training a model on a similar dataset improve the robustness of model–explanation pipelines? We fit linear regression on differences in alignment metric values to find the significant influence of model architectures and explanation methods on the robustness of model–explanation pipelines. Tables 5 & 6 show the coefficients and the corresponding p -values. We observe that signs of all coefficients are consistent between rank and mass accuracy. Vision transformers and SmoothGrad are, on average, less robust than DenseNet and vanilla gradient (baselines) respectively, which is also visible in Table 4. Crucially, the coefficient related to pre-training is negative, which shows that pre-training the model on RadImageNet improves the robustness of the model–explanation pipelines.

RQ4: Are model–explanation pipelines equally robust across different class labels of interest? In Figure 4, we perform a more detailed analysis of a particular model architecture (ViT). The top row shows a relationship between differences attributing to $\mathcal{R}_{\text{rank}}$ and $\mathcal{R}_{\text{mass}}$, where each dot corresponds to a data point evaluated on both aligned and misaligned model–explanation pipelines. We colour points with their corresponding class labels, i.e. lung pathologies.

	Coef.	Std. Err.	p -value
intercept	0.021	0.0023	$4.0e-19$
pre-trained model	-0.019	0.0018	$1.6e-26$
model: ViT	0.025	0.0021	$3.8e-31$
model: Swin-ViT	0.072	0.0022	$< 2.0e-32$
explanation: IG	0.029	0.0024	$3.4e-32$
explanation: SG	0.052	0.0025	$< 2.0e-32$
explanation: LRP	-0.030	0.0027	$2.2e-29$

Table 6: Coefficients of a linear regression model fitted to the differences of *rank accuracy* between aligned and misaligned model–explanation pipelines.

It shows that explanations for predicting Enlarged Cardio-mediastinum have the highest differences between the best and worst-case scenarios of alignment with human experts.

In the bottom row of Figure 4, we zoom into a particular model–explanation pipeline (ViT-IG). One can analyse each input image in detail to observe the possible change in explanations after (mis)alignment. In extreme cases (X-ray image in top right), it was possible to make explanations rather ambiguous, attributing the prediction to most of the features, even outside of the lung area.

5 Discussion and Related Work

In (Schramowski et al. 2020), the *localization* property of explanation methods is exploited to demonstrate that deep neural networks achieve high performance by using confounding features in data. An interactive process involving a human providing feedback on the model’s explanations shows how to align the model with human perception. We learned that it is possible to change the output of explanation methods without any drop in model performance (also shown by Heo, Joo, and Moon 2019).

We believe that explanations should be viewed as a proxy to understand predictive models (Samek et al. 2016). Therefore, the explanation’s quality with respect to localization would be hard to measure via human annotations. Instead, we can evaluate the model’s quality to localize accurate features by measuring the intersection between saliency maps and human annotations (Schramowski et al. 2020).

In (Watson, Shiekh Hasan, and Moubayed 2022), the localization property of explanation methods is used to evaluate the robustness of deep learning models with respect to the change in model architecture and hyperparameters. The study specifically focuses on medical imaging data and concludes with a concrete statement that the lack of explanation consistency is a fundamental problem with deep learning models rather than an issue with the localization property of explanations.

Contrary, Saporta et al. (2022) conclude that due to the low localization performance of explanation methods, we cannot rely on them for interpreting deep learning models in medical imaging. A natural question arises: **Can a low localization performance of explanation methods be put into question when deep learning models are inconsistent in the first place?**

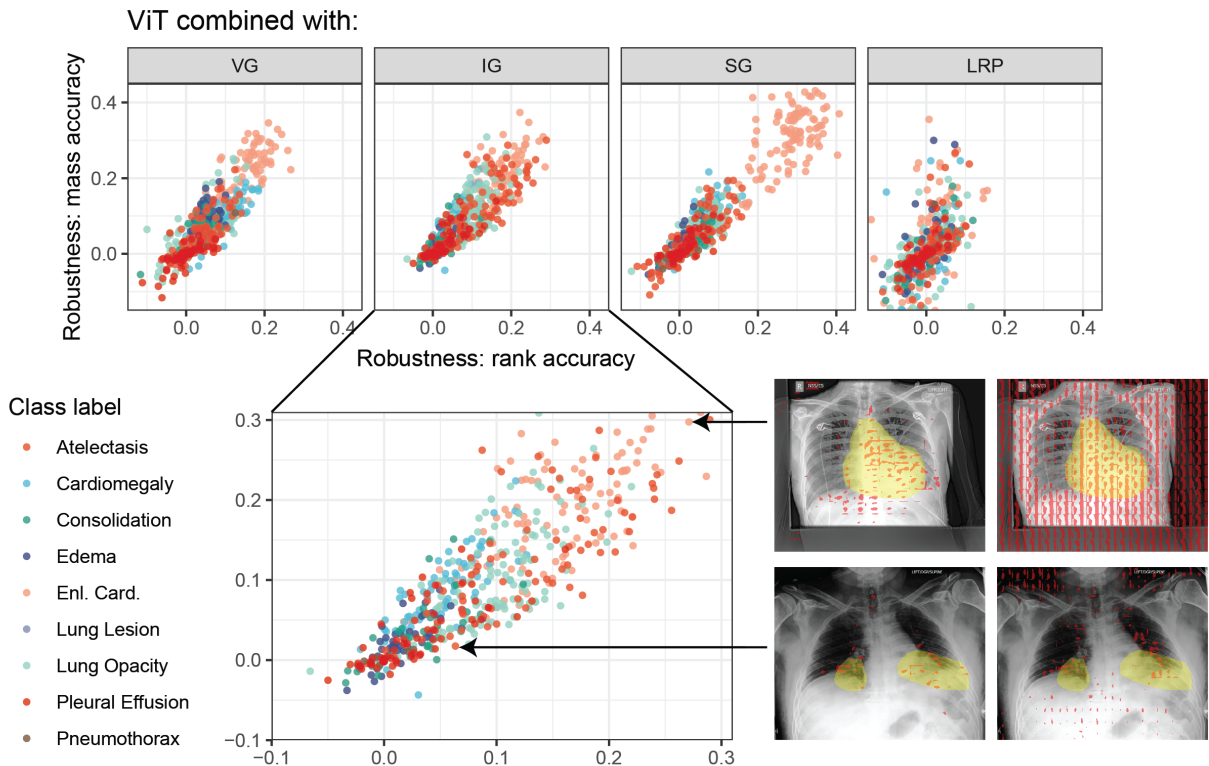


Figure 4: Analysis of robustness across different class labels for ViT. *Top row*: For each explanation method, we plot differences in rank and mass accuracy between aligned and misaligned pipelines. Each point corresponds to a single input image. *Bottom row*: Detailed analysis for the ViT-IG pipeline with a comparison between aligned and misaligned explanations for two patients.

Note that benchmarking the accuracy (i.e. localization performance in the case of explanation methods for image classification) of local post-hoc explanations against ground truth, either based on synthetic data or human annotations, is not a straightforward process. In scenarios considering structured/tabular data, it is possible to generate interpretable models for which the ground truth explanation is given by design (Guidotti 2021). Recently proposed approach to evaluating explanations regarding ground truth data considers enforcing complex constraints on the data generating process (see Agarwal et al. 2022, Appendix C).

However, in scenarios considering high-dimensional unstructured data, the assumption that a model has to use features perceived by humans as important is not always true. In (Faber, K. Moghaddam, and Wattenhofer 2021), a set of experiments shows that deep neural networks may not necessarily use important features encoded in synthetic datasets for making predictions. Therefore, synthetically made ground truth ought to be used with caution when benchmarking explanations. In (Makino et al. 2022), a set of experiments involving a medical imaging task and human annotators specifically show that deep neural networks perceive different features as important than humans. In many cases, this is a desirable property as various stakeholders may use machine learning to receive model-driven feedback about the unknown correlation structure in data.

Finally, we ought to point out the work of (Arun et al. 2021), which also evaluates (among others) the localization utility of explanation methods for chest X-ray interpretation by comparing them with segmentation models, which could be understood as *more appropriate*.

In evidence of related work (Schramowski et al. 2020; Faber, K. Moghaddam, and Wattenhofer 2021; Watson, Shiekh Hasan, and Moubayed 2022; Makino et al. 2022), we cannot assume that the models we use dominantly base their decision on features of human interest, especially in the case of complex medical images. **We sincerely hope that practitioners actually use best-performing explanation methods to assess the trustworthiness of learning algorithms**, e.g. by being careful when model predictions of cancer are based on features in the background of an image.

6 Conclusion

We caution practitioners to be careful when evaluating explanations regarding ground truth, especially when it’s defined by human perception. As shown in our experiments, the focus of these benchmarks is primarily on evaluating the quality of the model–explanation pipelines under consideration, rather than examining the interpretation methods themselves. The introduced framework should be used to evaluate the robustness of AI systems, whenever the goal is to achieve alignment with human expertise.

Reproducibility

Code used to reproduce all of the experimental results will be available at <https://github.com/mi2datalab/be-careful-evaluating-explanations>. The datasets used are openly available at <https://stanfordmlgroup.github.io/competitions/chexpert> and <https://stanfordaimi.azurewebsites.net/datasets/23c56a0d-15de-405b-87c8-99c30138950c>.

We acknowledge the differences between baseline values reported in Table 1 and values of AUC, Hit-rate, and mIoU reported in (Saporta et al. 2022). We attribute it to the possible differences in the implementation of model training and explanation computation. However, the demonstrated gap between the three scenarios is, in general, implementation-agnostic.

References

- Adebayo, J.; Muelly, M.; Abelson, H.; and Kim, B. 2022. Post hoc Explanations may be Ineffective for Detecting Unknown Spurious Correlation. In *ICLR*.
- Agarwal, C.; Krishna, S.; Saxena, E.; Pawelczyk, M.; Johnson, N.; Puri, I.; Zitnik, M.; and Lakkaraju, H. 2022. OpenXAI: Towards a Transparent Evaluation of Model Explanations. In *NeurIPS*.
- Ali, A.; Schnake, T.; Eberle, O.; Montavon, G.; Müller, K.-R.; and Wolf, L. 2022. XAI for Transformers: Better Explanations through Conservative Propagation. In *ICML*.
- Arora, S.; Pruthi, D.; Sadeh, N.; Cohen, W. W.; Lipton, Z. C.; and Neubig, G. 2022. Explain, Edit, and Understand: Rethinking User Study Design for Evaluating Model Explanations. In *AAAI*.
- Arras, L.; Osman, A.; and Samek, W. 2022. CLEVR-XAI: A benchmark dataset for the ground truth evaluation of neural network explanations. *Information Fusion*, 81: 14–40.
- Arun, N.; Gaw, N.; Singh, P.; Chang, K.; Aggarwal, M.; Chen, B.; Hoebel, K.; Gupta, S.; Patel, J.; Gidwani, M.; et al. 2021. Assessing the trustworthiness of saliency maps for localizing abnormalities in medical imaging. *Radiology: Artificial Intelligence*, 3(6).
- Bach, S.; Binder, A.; Montavon, G.; Klauschen, F.; Müller, K.-R.; and Samek, W. 2015. On pixel-wise explanations for non-linear classifier decisions by layer-wise relevance propagation. *PloS one*, 10(7): e0130140.
- Bhatt, U.; Weller, A.; and Moura, J. M. F. 2020. Evaluating and Aggregating Feature-based Model Explanations. In *IJCAI*.
- Dai, J.; Upadhyay, S.; Aivodji, U.; Bach, S. H.; and Lakkaraju, H. 2022. Fairness via Explanation Quality: Evaluating Disparities in the Quality of Post Hoc Explanations. In *AIES*.
- Dosovitskiy, A.; Beyer, L.; Kolesnikov, A.; Weissenborn, D.; Zhai, X.; et al. 2021. An Image is Worth 16x16 Words: Transformers for Image Recognition at Scale. In *ICLR*.
- Faber, L.; K. Moghaddam, A.; and Wattenhofer, R. 2021. When Comparing to Ground Truth is Wrong: On Evaluating GNN Explanation Methods. In *KDD*.
- Guidotti, R. 2021. Evaluating local explanation methods on ground truth. *Artificial Intelligence*, 291: 103428.
- Guidotti, R.; Monreale, A.; Matwin, S.; and Pedreschi, D. 2020. Explaining Image Classifiers Generating Exemplars and Counter-Exemplars from Latent Representations. In *AAAI*.
- Heo, J.; Joo, S.; and Moon, T. 2019. Fooling Neural Network Interpretations via Adversarial Model Manipulation. In *NeurIPS*.
- Holzinger, A.; Haibe-Kains, B.; and Jurisica, I. 2019. Why imaging data alone is not enough: AI-based integration of imaging, omics, and clinical data. *European Journal of Nuclear Medicine and Molecular Imaging*, 46(13): 2722–2730.
- Huang, G.; Liu, Z.; Pleiss, G.; Maaten, L. v. d.; and Weinberger, K. Q. 2019. Convolutional Networks with Dense Connectivity. *IEEE Transactions on Pattern Analysis and Machine Intelligence*, 44(12): 8704–8716.
- Irvin, J.; Rajpurkar, P.; Ko, M.; Yu, Y.; Ciurea-Ilicus, S.; et al. 2019. CheXpert: A Large Chest Radiograph Dataset with Uncertainty Labels and Expert Comparison. In *AAAI*.
- Joo, S.; Jeong, S.; Heo, J.; Weller, A.; and Moon, T. 2023. Towards More Robust Interpretation via Local Gradient Alignment. In *AAAI*.
- Komorowski, P.; Baniecki, H.; and Biecek, P. 2023. Towards Evaluating Explanations of Vision Transformers for Medical Imaging. In *CVPR*.
- Liu, Z.; Lin, Y.; Cao, Y.; Hu, H.; Wei, Y.; Zhang, Z.; Lin, S.; and Guo, B. 2021. Swin Transformer: Hierarchical Vision Transformer Using Shifted Windows. In *ICCV*.
- Makino, T.; Jastrzebski, S.; Oleszkiewicz, W.; Chacko, C.; Ehrenpreis, R.; Samreen, N.; Chhor, C.; Kim, E.; Lee, J.; Pysarenko, K.; et al. 2022. Differences between human and machine perception in medical diagnosis. *Scientific Reports*, 12(1): 1–13.
- Mei, X.; Liu, Z.; Robson, P. M.; Marinelli, B.; Huang, M.; Doshi, A.; Jacobi, A.; Cao, C.; Link, K. E.; Yang, T.; Wang, Y.; Greenspan, H.; Deyer, T.; Fayad, Z. A.; and Yang, Y. 2022. RadImageNet: An Open Radiologic Deep Learning Research Dataset for Effective Transfer Learning. *Radiology: Artificial Intelligence*, 4(5): e210315.
- Ridnik, T.; Ben-Baruch, E.; Noy, A.; and Zelnik, L. 2021. ImageNet-21K Pretraining for the Masses. In *NeurIPS*.
- Rudin, C. 2019. Stop explaining black box machine learning models for high stakes decisions and use interpretable models instead. *Nature Machine Intelligence*, 1(5): 206–215.
- Samek, W.; Binder, A.; Montavon, G.; Lapuschkin, S.; and Müller, K.-R. 2016. Evaluating the visualization of what a deep neural network has learned. *IEEE Transactions on Neural Networks and Learning Systems*, 28(11): 2660–2673.
- Saporta, A.; Gui, X.; Agrawal, A.; Pareek, A.; Truong, S. Q.; Nguyen, C. D.; Ngo, V.-D.; Seekins, J.; Blankenberg, F. G.; Ng, A. Y.; et al. 2022. Benchmarking saliency methods for chest X-ray interpretation. *Nature Machine Intelligence*, 4: 867–878.

Schramowski, P.; Stammer, W.; Teso, S.; Brugger, A.; Herbert, F.; Shao, X.; Luigs, H.-G.; Mahlein, A.-K.; and Kersting, K. 2020. Making deep neural networks right for the right scientific reasons by interacting with their explanations. *Nature Machine Intelligence*, 2(8): 476–486.

Selvaraju, R. R.; Cogswell, M.; Das, A.; Vedantam, R.; Parikh, D.; and Batra, D. 2019. Grad-CAM: Visual Explanations from Deep Networks via Gradient-Based Localization. *International Journal of Computer Vision*, 128(2): 336–359.

Shrotri, A. A.; Narodytska, N.; Ignatiev, A.; Meel, K. S.; Marques-Silva, J.; and Vardi, M. Y. 2022. Constraint-Driven Explanations for Black-Box ML Models. In *AAAI*.

Simonyan, K.; Vedaldi, A.; and Zisserman, A. 2014. Deep Inside Convolutional Networks: Visualising Image Classification Models and Saliency Maps. In *ICLR*.

Smilkov, D.; Thorat, N.; Kim, B.; Viégas, F.; and Wattenberg, M. 2017. SmoothGrad: removing noise by adding noise. *arXiv:1706.03825*.

Sundararajan, M.; Taly, A.; and Yan, Q. 2017. Axiomatic Attribution for Deep Networks. In *ICML*.

Tomsett, R.; Harborne, D.; Chakraborty, S.; Gurram, P.; and Preece, A. 2020. Sanity Checks for Saliency Metrics. In *AAAI*.

Watson, M.; Shiekh Hasan, B. A.; and Moubayed, N. A. 2022. Agree to Disagree: When Deep Learning Models With Identical Architectures Produce Distinct Explanations. In *WACV*.

Zhou, Y.; Booth, S.; Ribeiro, M. T.; and Shah, J. 2022. Do Feature Attribution Methods Correctly Attribute Features? In *AAAI*.

A Experimental Setup

Dataset. In experiments, we use four subsets of data: two derived from the CheXpert dataset (Irvin et al. 2019) and two from the CheXlocalize dataset (Saporta et al. 2022). Table 7 shows the distribution of class labels for each subset. Note that only 10 out of 14 class labels appearing in CheXpert have ground truth masks in CheXlocalize (missing: fracture, pleural other, pneumonia, no finding). In experiments, we omit the additional class denoting support devices and use the remaining 9 lung pathologies with ground truth masks. For further details refer to the original articles (Irvin et al. 2019; Saporta et al. 2022).

We divide the CheXpert training set into two subsets for training models (named **Training** and **Validation** in Table 7). We do so because the original CheXpert validation set is the same as CheXlocalize, and we cannot use it during training before the evaluation of (mis)aligned model–explanation pipelines. For fine-tuning the alignment of model–explanation pipelines, we use the CheXlocalize test set (named **Fine-tuning** in Table 7). We measure alignment metrics and robustness on the validation set of CheXlocalize (named **Validation** in Table 7). Thus, the four sets of images are disjoint.

Models. We train all models using images resized to the size of (224×224) , normalized to the range $[-1, 1]$, and augmented with random rotations in the range of $(-15, 15)$ degrees. We use the AdamW optimizer. For Transformer models, we use a cosine learning rate schedule with 2000 warmup steps. In each experiment, the base learning rate is set to $1e-4$ and the batch size to 128. We train each model on a single random seed.

B Additional Results

RQ1: How robust are convolutional neural networks and vision transformers combined with various explanation methods? See Figures 5, 6, 7.

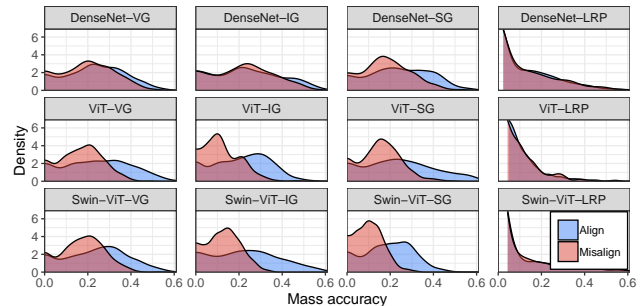


Figure 5: Distribution of *mass accuracy* values for the *pre-trained* model–explanation pipelines.

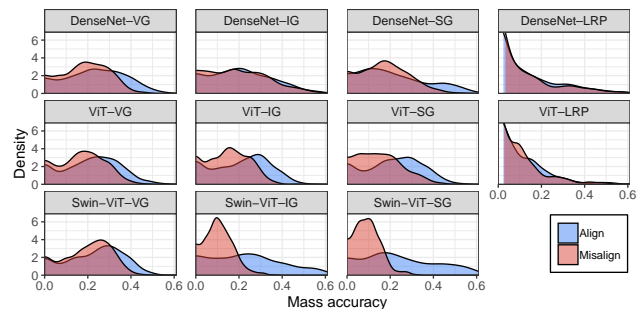


Figure 6: Distribution of *mass accuracy* values for the *non-pre-trained* model–explanation pipelines.

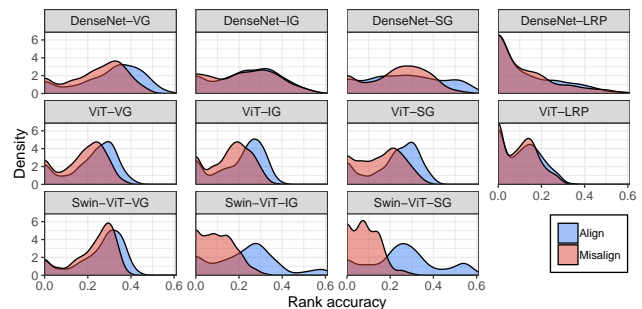


Figure 7: Distribution of *rank accuracy* values for the *non-pre-trained* model–explanation pipelines.

Class label	CheXpert (Irvin et al. 2019)				CheXlocalize (Saporta et al. 2022)			
	Training		Validation		Fine-tuning		Validation	
	Negative	Positive	Negative	Positive	Negative	Positive	Negative	Positive
Atelectasis	186076	33253	3476	609	490	178	154	80
Cardiomegaly	189342	29987	3506	579	493	175	166	68
Consolidation	205881	13448	3851	234	633	35	201	33
Edema	167321	52008	3035	1050	583	85	189	45
Enl. Card.	211840	7489	3963	122	370	298	125	109
Fracture	210765	8564	3948	137	662	6	234	0
Lung Lesion	210120	9209	3948	137	654	14	233	1
Lung Opacity	118092	101237	2230	1855	358	310	108	126
No Finding	198669	20660	3621	464	559	109	196	38
Pleural Effusion	131692	87637	2408	1677	548	120	167	67
Pleural Other	215451	3878	4004	81	660	8	233	1
Pneumonia	214553	4776	4005	80	654	14	226	8
Pneumothorax	201745	17584	3800	285	658	10	226	8
Support Devices	108302	111027	1977	2108	353	315	127	107

Table 7: Class label counts in the four disjoint dataset subsets used in experiments. Only 10 out of 14 class labels appearing in CheXpert have ground truth masks in CheXlocalize (missing: Fracture, Pleural Other, Pneumonia, No Finding).